

利用鈷鈦催化金屬合成柱狀結構之奈米碳管之場發射特性的研究

研究生：林君翰

指導教授：鄭晃忠 博士

國立交通大學電機學院產業研發碩士班

摘 要

本論文主要是針對柱狀結構之奈米碳管場發射陣列進行其場發射特性的研究。由於奈米碳管具有奈米級的管徑，極大的高寬比，堅強的機械性質及穩定的化學性質，因此，一直是極具潛力的場發射顯示器材料。由場發射的測試中，發現奈米碳管具有非常優異的場發射特性；我們利用熱化學氣相沉積系統進行奈米碳管的合成，可惜其密度很高 ($10^9 \sim 10^{10}/\text{cm}^2$)，而密度較高的奈米碳管因為電場之遮蔽效應(screening effect)使得其場發射特性並不因其具有較高密度之場發射源而變好；另外，因為電場的遮蔽效應，柱狀結構之奈米碳管僅有其周圍的奈米碳管會發射電子，因此，我們嘗試成長柱狀型態的碳管陣列，經由成長條件之控制，調變陣列間距與碳管長度的比值，我們發現雖然每個柱狀的碳管密度都很高，但是卻具有極佳的場發射特性。

本論文首先進行柱狀結構之奈米碳管場發射陣列的成長，發現鈷鈦雙層催化金屬 (Co/Ti Bi-layered catalyst films) 前處理後的顆粒比使用鐵鈦或鎳鈦做催化金屬的顆粒來的小而且均勻，因為催化金屬顆粒均勻可使奈米碳管成長的速率相同，因此，我們順利的利用鈷鈦雙層催化金屬合成高度相當一致的奈米碳管柱狀結構之奈米碳管場發射陣列。

另外，我們使用鈷鈦催化金屬所合成柱狀結構的奈米碳管，並且利用微影的方法來控制柱體和柱體之間的距離以及柱體高度來降低電場遮蔽效應，獲得最佳的場發射特性。根據本實驗，我們發現場發射電流密度與奈米碳管場發射陣列的周長大小有一定比

例的關連;再討論到不同柱體間距時,我們發現最佳的場發射特性存在於R/H Ratio(柱體間距與柱體高度的比值)為 2.041 時,其起始電場(turn on field)是 0.808 V/ μm ,電流密度(current density)也高達 900.1 mA/ cm^2 ,並且在固定電場 4.33 V/ μm 一小時裡,場發射的可靠度亦相當良好,電流的變異大約為 6.52 %,其平均電流密度約 18.4 mA/ cm^2 ,並且在塗佈螢光粉之陽極板上得到均勻之光源,因此,這種鈷鈦催化金屬合成的柱狀結構奈米碳管,具有相當潛力來應用在薄膜電晶體液晶顯示器上的背光源,以有效地降低製造材料成本。



Study on the Field Emission Characteristics of Carbon-Nanotubes Pillar Arrays Using Co/Ti Bi-Layered Catalyst

Student : Jun-Han Lin Advisor : Dr. Huang-Chung Cheng

Industrial Technology R & D Master Program of
Electrical and Computer Engineering College
National Chiao Tung University

Abstract

In this thesis, we focus our study on the field emission characteristics of carbon-nanotube (CNTs) pillar arrays. Due to CNTs' high aspect ratio, well chemical stability, high mechanical strength and small radii of curvature, carbon nanotubes have become the hot material for field emission display. Thermal chemical vapor deposition (TCVD) is used to grow the carbon nanotubes. However, the density of grown CNTs is still very high ($10^9 \sim 10^{10}$) and is difficult to be controlled. Besides, the electric field is screened because of the closely spaced CNTs, which results in a reduced effective electric field near the CNT emitters. As a result, turn-on electric field increases and emission current density decreases. To obtain the better field emission properties, the density of CNTs should be optimized.

The periphery of the carbon nanotube pillar plays a dominant role on the field emission effect and act as a major emission sites. Then the screen effect of CNTs can be controlled via the lithography-patterned structure of CNT pillar arrays. Therefore the CNT pillar array scheme is not only an effective way to reduce the complexity in processes but also a cost effective way to reduce the cost.

It is reported that uniform size of nanoparticles can easily grow CNTs with the same rate. Therefore, we first study the pretreatment of catalytic film including Ni/Ti, Fe/Ti, and Co/Ti as well as find that nanoparticles obtained by Co/Ti bi-layered are uniform in size and smaller than the other two bi-layered catalysts. We finally grow CNT pillar arrays with uniform length by properly controlling the growth parameters using Co/Ti bi-layered catalyst.

Then, we utilize the proposed method to synthesize CNT pillar arrays to reduce the screening effect via the pillar density design. In our study, we have found that the field emission current density is relevant to the perimeters of the field emission arrays. Finally, by adjusting the inter-pillar distance (R) and height (H) of CNT pillars, the optimization of the field emission characteristics can be obtained. According to our study, the optimum of the field emission is found at R/H ratio of 2.041. The effective turn-on field is as low as 0.808 V/ μm . The maximum current density is as high as 900.1 mA/cm². The reliability of the pillar arrays is also determined by a stress test at 4.33 V/ μm for 1 hour. Those results show an excellent reliability for the CNT pillars with the current variation coefficient of 6.52 %, and average current density of 18.4 mA/cm² after the stress. A homogeneous light emission is also observed on the phosphor (P22) coated glasses. As a result, CNT pillars arrays are a potential candidate in the application of the back light unit for TFT-LCDs.

Contents

Abstract (in Chinese)	i
Abstract (in English)	iii
Acknowledgments (in Chinese)	vi
Contents	v
Table Lists	viii
Figure Captions	ix

Chapter 1 Introduction

1.1 <i>Overview of Vacuum Microelectronics</i>	1
1.1.1 History.....	1
1.1.2 Applications of Vacuum Microelectronics.....	3
1.1.3 Field Emission Displays.....	5
1.2 <i>Materials and Structures of Cathode for Field Emission Displays</i>	6
1.2.1 Theory Background.....	6
1.2.2 Spindt-type Field Emission.....	10
1.2.3 BSD Field Emission.....	12
1.2.4 MIM Field Emission.....	13
1.2.5 Carbon and Nano-sized Field Emission.....	13
1.2.6 Surface Conduction Electron Emission (SCE).....	14
1.3 <i>Synthesis Methods and Field Emission Properties of Carbon Nanotubes</i>	14
1.3.1 Structure of Carbon Nanotubes.....	15
1.3.2 Physical and Chemical Properties of Carbon Nanotubes.....	16
1.3.3 The Synthesis Methods of Carbon Nanotubes.....	17
1.3.4 Potential Application of Carbon Nanotube.....	18
1.4 <i>Thesis Organization</i>	19

Chapter 2 Experimental Procedures

2.1 Motivation.....	21
2.2 Growth of Carbon Nanotubes Pillar Arrays Using Ni /Ti, Fe/Ti and Co/Ti Bi-Layered Catalysts.....	23
2.2.1 Forward Arrangement.....	23
2.2.2 Experimental Procedures.....	24
2.3 Field Emission Characteristics with Different Array's Edges.....	25
2.3.1 Pixel Design.....	25
2.3.2 CNTs Synthesis.....	26
Experiment Condition.....	26
2.3.3 Different Temperature.....	27
2.3.4 Co versus Fe.....	27
2.4 Field Emission Characteristics with Different Inter-Pillar Distances.....	27
2.4.1 Inter-Pillar Distance Design.....	28
2.4.2 CNTs Synthesis.....	28
2.5 Analysis.....	28

Chapter 3 Results and Discussion

3.1 Growth of Carbon Nanotubes Pillar Arrays Using Ni/Ti, Fe/Ti and Co/Ti Bi-Layered Catalysts.....	30
3.1.1 Effect of H ₂ pretreatment on Ni /Ti and Fe/Ti bi-layered catalysts.....	31
3.1.2 Effect of growth time on the morphology of CNTs grown by Fe/Ti bi-layered catalysts.....	33
3.1.3 Effect of carbon source flow rates on the morphology of CNTs grown by Fe/Ti catalyst.....	34
3.1.4 Effect of H ₂ pretreatment on Co/Ti bi-layered catalysts.....	35
3.1.5 Effect of growth time on the morphology of CNTs grown by Co/Ti bi-layered catalysts.....	36
3.1.6 Effect of growth temperature on the morphology of CNTs grown by Co/Ti bi-layered catalysts.....	37
3.1.7 SEM and TEM micrographs' comparison of CNTs grown using (a) Co/Ti (b) Fe/Ti (c) Ni/Ti bi-layered catalyst.....	38
3.2 The relation between field emission characteristics and perimeter of the field emission.....	

<i>arrays</i>	38
3.2.1 Pixel design.....	39
3.2.2 Optimal growth condition.....	40
3.2.3 Comparison of morphology and field emission characteristics of CNTs grown by Co catalyst with that by Fe catalyst.....	42
3.3 Field emission characteristics with different R/H ratios	43
3.3.1 Different R/H Ratios with 40um Inter Pillar Distance.....	44
3.3.2 Different R/H Ratios with 60um Inter Pillar Distance.....	44
3.3.3 Different R/H Ratios with 100um Inter Pillar Distance.....	44
3.4 Comparison of Experimental Results with Simulation Results to the Effect of R/H Ratios on Field Emission Current Density	45
3.4.1 Different R/H Ratios with CNTs' Length is Fixed at 10um.....	45
3.4.2 Different R/H Ratios with CNTs' Length is Fixed at 34um.....	46
3.4.3 Comparison Result between Experimental and Simulation Results.....	46
Chapter 4 Summary and Conclusions	
<i>4.1 Summary and Conclusions</i>	48
Tables	51
Figures	56
References	101
Vita	107



Table Lists

Chapter 1

Table 1-1 Comparison between vacuum microelectronics and solid-state electronics.....51

Chapter 3

Table 3-1 Comparisons of turn-on field, threshold field and emission current density at 6.67 V/ μms of CNTs between small, middle, and large sizes of pillar arrays. Table 3-2 Field emission properties of CNTs with different spacing between pillars at 800 V for 1 hour.....52

Table 3-2 Experimental design of CNTs synthetic conditions of finding the optimum growth condition.....53

Table 3-3 Comparisons of turn-on field, threshold field and emission current density at 6.67 V/ μm of CNTs between CNTs synthetic conditions in our experimental design.....54

Table 3-4 Comparison of field emission current fluctuation at 650 V between CNTs grown by Co catalyst and CNTs grown by Fe catalyst.....55

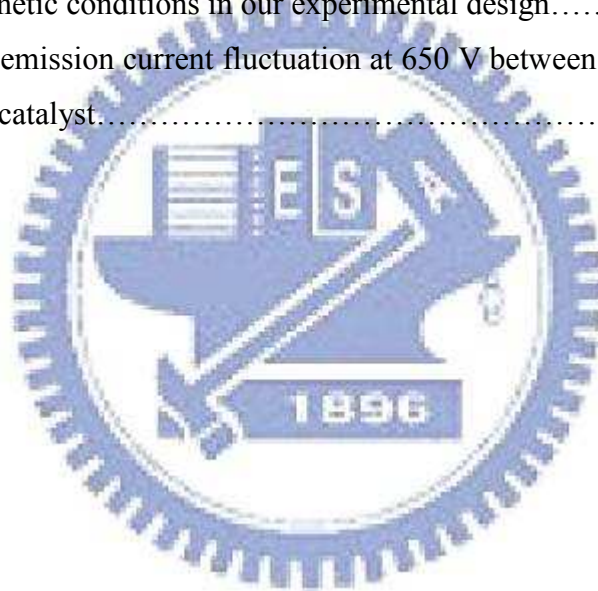


Figure Captions

Chapter 1

Figure 1-1 The SEM micrograph of (a) Spindt type triodes array, (b) Spindt type field emission triode.....	56
Figure 1-2 The schematic diagram of (a) conventional CRT and (b) FED.....	57
Figure 1-3 Energy diagrams of vacuum-metal boundary:.....	58
(a) without external electric field;	
(b) with an external electric field.	
Figure 1-4 The full color FED products: (a) Pixtech 5.6” color FED based on Spindt-type, (b) Futaba 7” color FED based on Spindt-type, (c) Sony/Candescent 13.2” color FED based on Spindt-type and (d) Canon-Toshiba 36” SED-TV.....	59
Figure 1-5 This diagram is the field emission mechanism of BSD.....	60
Figure 1-6 Structures of carbon (a) graphite (b) diamond and (c) fullerene.....	61
Figure 1-7 TEM images of (a) SWNT and (b) MWNT.....	62
Figure 1-8 Growth mechanism of CNTs growth (a) base growth model and (b) tip growth model.....	63

Chapter 2

Figure 2-1 experiment procedures.....	64
Figure 2-2 (a) Simulation of the equipotential lines of the electrostatic field for tubes of 1 μm height and 2 nm radius, for distances between tubes of 4, 1, and 0.5 μm ; along with the corresponding changes of the field enhancement factor β and emitter density (b), and current density (c) as a function of the distance.....	65
(Ref. Appl. Phys. Lett. 76 (2000) 2071)	
Figure 2-3 (a) Field amplification factor β as a function of the onset field after training, E_i , for the films obtained by CVD with different catalyst concentrations, (b) Low current field emission characteristics of the 11 samples after training.....	66
(Ref. Carbon 40 (2002) 1715)	
Figure 2-4 Growth condition of CNT pillars in the thermal CVD system.....	67
Figure 2-5 Growth condition of CNT pillars in the thermal CVD system.....	68
Figure 2-6 Growth condition of CNT pillars in the thermal CVD system.....	69
Figure 2-7 (a) Emission Area: $20 \times 20 \times 50 \times 50 = 10^6 \mu\text{m}^2$ Perimeter: $80 \times 2500 = 2 \times 10^5 \mu\text{m}$ (b) Emission Area: $200 \times 200 \times 5 \times 5 = 10^6 \mu\text{m}^2$ Perimeter: $800 \times 25 = 2 \times 10^4 \mu\text{m}$ (c) Emission Area: $1000 \times 1000 = 10^6 \mu\text{m}^2$ Perimeter: $4 \times 10^3 \mu\text{m}$, the Perimeter ratios = 50 : 5 : 1.....	70

Figure 2-8 (a) photo and (b) schematic picture of thermal CVD.....	71
Figure 2-9 Experimental procedures for CNT pillars synthesized.....	72
Figure 2-10 (a)Pixel Area: $8.8 \times 10^6 \mu\text{m}^2$ (b)Pixel Area: $15.5 \times 10^6 \mu\text{m}^2$ (c)Pixel Area: $34.8 \times 10^6 \mu\text{m}^2$	73
Figure 2-11 Schematic diagram of a high-vacuum system setup for field emission measurement.....	74

Chapter 3

Figure 3-1 SEM and AFM micrographs of Ni /Ti bi-layered catalysts pre-treated in N_2/H_2 gas mixtures with different hydrogen flow rates.....	75
Figure 3-2 SEM and AFM micrographs of Fe/Ti bi-layered catalysts pre-treated in N_2/H_2 gas mixtures with different hydrogen flow rates.....	76
Figure 3-3 The typical SEM image using Fe/Ti bi-layered as catalysts for CNTs growth.....	77
(a) Growth condition: $700 \text{ }^\circ\text{C}$, Pretreatment: $\text{N}_2/\text{H}_2=500/500$, 15min, Growth: $\text{N}_2/\text{H}_2/\text{C}_2\text{H}_4=500/0/40$, 9min.	
(b) Growth condition: $700 \text{ }^\circ\text{C}$ Pretreatment: $\text{N}_2/\text{H}_2=500/130$, 15min, Growth: $\text{N}_2/\text{H}_2/\text{C}_2\text{H}_4=500/100/20$, 15min.	
Figure 3-4 Effect of Growth time on the morphology of CNTs grown by Fe/Ti catalyst (a) 15min (b) 45min, Growth condition: $700 \text{ }^\circ\text{C}$, Pretreatment: $\text{N}_2/\text{H}_2=500/100$, 15min, Growth: $\text{N}_2/\text{H}_2/\text{C}_2\text{H}_4=500/100/20$	78
Figure 3-5 Effect of carbon source on the morphology of CNTs grown by Fe/Ti catalyst. Growth condition : $700 \text{ }^\circ\text{C}$, Pretreatment: $\text{N}_2/\text{H}_2=500/100$,15min, Growth: (a) $\text{N}_2/\text{H}_2/\text{C}_2\text{H}_4=500/100/20$ (b) $\text{N}_2/\text{H}_2/\text{C}_2\text{H}_4=500/100/40$	79
Figure 3-6 SEM and AFM micrographs of Co /Ti bi-layered catalysts pre-treated in N_2/H_2 gas mixtures with different hydrogen flow rates.....	80
Figure 3-7 Effect of growth time on the morphology of CNTs grown by Co/Ti catalyst (a) 15min (b) 45min, Growth condition 700 , Pretreatment: $\text{N}_2/\text{H}_2=500/100$, 15min, Growth: $\text{N}_2/\text{H}_2/\text{C}_2\text{H}_4=500/100/20$	81
Figure 3-8 SEM micrographs of Co /Ti bi-layered catalysts pre-treated in N_2/H_2 gas mixtures with different growth temperatures and their morphology of CNTs.....	82
Figure 3-9 SEM and TEM micrographs of CNTs grown using (a) Co/Ti, (b) Fe/Ti and (c) Ni/Ti bi-layered catalyst.....	83
Figure 3-10 SEM micrographs of small, middle, and large sizes of CNTs' pixel arrays.....	84
Figure 3-11 Field emission characteristics for small, middle, and large sizes of CNTs' arrays.....	85
Figure 3-12 SEM micrographs of CNTs synthetic conditions in our experimental design.....	86

Figure 3-13 Raman and I-V plot in the experimental design of CNTs synthetic conditions.....	87
Figure 3-14 Comparison of morphology and field emission characteristics of CNTs grown by Co with that by Fe catalyst.....	88
Figure 3-15 Field emission stability at 650 V and emission image of CNTs grown by Co and CNTs grown by Fe.....	89
Figure 3-16 Different R/H ratios with 40 μm inter pillar distance.....	90
Figure 3-17 Field emission characteristics of different R/H ratios with 40 μm inter pillar distance.....	91
Figure 3-18 Different R/H ratios with 60 μm inter pillar distance.....	92
Figure 3-19 Field emission characteristics of different R/H ratios with 60 μm inter pillar distance.....	93
Figure 3-20 Different R/H ratios with 100 μm inter pillar distance.....	94
Figure 3-21 Field emission characteristics of different R/H ratios with 100 μm inter pillar distance.....	95
Figure 3-22 SEM micrograph of different R/H ratios with CNTs' length is fixed at 10 μm	96
Figure 3-23 Field emission characteristics of different R/H ratios with CNTs' length is fixed at 10 μm	97
Figure 3-24 SEM micrograph of different R/H ratios with CNTs' length is fixed at 34 μm	98
Figure 3-25 Field emission characteristics of different R/H ratios with CNTs' length is fixed at 34 μm	99
Figure 3-26 Comparison of experimental results with simulation results to the effect of R/H ratios on field emission current at 7.4 V/ μm	100

